Available online at www.sciencedirect.com

ScienceDirect

Journal of the European Ceramic Society 34 (2014) 4235–4245

www.elsevier.com/locate/jeurceramsoc

Temperature-insensitive large electrostrains and electric field induced intermediate phases in $(0.7-x)Bi(Mg_{1/2}Ti_{1/2})O_3$–$xPb(Mg_{1/3}Nb_{2/3})O_3$–$0.3PbTiO_3$ ceramics

Wanli Zhao, Ruzhong Zuo *, Jian Fu

Institute of Electro Ceramics & Devices, School of Materials Science and Engineering, Hefei University of Technology, Hefei 230009, PR China

Received 1 June 2014; received in revised form 10 July 2014; accepted 12 July 2014
Available online 28 July 2014

Abstract

Large electrostrains (~0.4% at 7 kV/mm) of the new $(0.7-x)Bi(Mg_{1/2}Ti_{1/2})O_3$–$xPb(Mg_{1/3}Nb_{2/3})O_3$–$0.3PbTiO_3$ ($(0.7-x)$BMT–xPMN–0.3PT) ceramics with $x = 0.0$–0.7 near the morphotropic phase boundary of the BMT–PT–PMN ternary system were found to be associated with the evolution of the compositionally modulated dielectric relaxor behavior. As disclosed by in situ high-resolution synchrotron X-ray diffraction, more intermediate phases of different symmetries induced by external fields largely contribute to smaller strain hysteresis (~23%) of PMN-rich compositions than BMT-rich ones. Particularly, the $x = 0.2$ sample exhibits temperature-insensitive electrostrains of ~0.3% at 5 kV/mm varying less than 10% from room temperature up to 160 °C, which is mainly attributed to the coexistence of two kinds of relaxor states in a broad temperature range owing to special static domain structures typical for BMT-rich compositions. These findings provide a new approach toward an appropriate compositional design for low-hysteresis temperature-insensitive large electrostrains in BMT-based relaxor ferroelectrics.

Keywords: Perovskites; Relaxor; Strain; Temperature insensitivity; Low hysteresis

1. Introduction

Ferroelectric ceramics have been widely used as actuators, sensors, and transducers over the last several decades.[1,2] However, the commercial $Pb(Zr,Ti)O_3$ (PZT)-based ferroelectric ceramics usually have a relatively low electrostrain (<0.2%), although they could achieve enhanced intrinsic contributions to strains by means of the field induced inter-ferroelectric phase transformation.[3–5] $PbZrO_3$ (PZ)-based antiferroelectric ceramics are capable of generating large strains through a considerable volume variation involved in the field induced antiferroelectric-to-ferroelectric phase transition.[6] How to couple the piezoelectric effect with a strain-generating phase transition and at the same time to extend opportunities for actuator applications in a completely new manner would be of much interest from the viewpoint of the material design.

Large electrostrains (~0.4%) have been reported in recent years in a few bismuth-containing perovskite compounds upon the application of a high external electric field.[7–9] The generation of large strains was usually found to be associated with the formation of a weak relaxor behavior.[9] Relaxors were known to own giant dielectric and electromechanical responses, whose intrinsic inhomogeneities play a crucial role in inducing colossal effects. Such complex physical phenomena open new avenues for designing large-strain actuator materials. The recently-reported $(Bi_{1/2}Na_{1/2})TiO_3$ (BNT)-based relaxors are typical examples exhibiting a large electric-field-induced strain when the high-temperature polymorphism is shifted down to room temperature after the compositional modification.[10] It was later on considered as a consequence of the electric field induced polar to nonpolar phase transition, as found in canonical relaxors $Pb(Mg_{1/3}Nb_{2/3})O_3$ (PMN) or La-doped PZT.[11,12] In the family of bismuth-containing perovskite compounds, $Bi(Mg_{1/2}Ti_{1/2})O_3$ (BMT) should be one outstanding candidate since it was widely investigated as high-temperature piezoelectric materials.[13,14] The activation of its special static domains

* Corresponding author. Tel.: +86 551 62905285; fax: +86 551 62905285.
E-mail addresses: piezolab@hfut.edu.cn, rzzuo@hotmail.com (R. Zuo).

http://dx.doi.org/10.1016/j.jeurceramsoc.2014.07.017
0955-2219/

through the addition of a small amount of second phases such as $BaZrO_3$, PZ and so on can induce similar large-strain behavior in BMT-PT ternary system.[9,15,16] These electric field induced large strains are usually observed in a very narrow composition or temperature window, and exhibit severe hysteresis, thus limiting their usages for practical applications. Although the temperature stability of strain in BNT-based ceramics was believed to be slightly better than Pb-based relaxors,[17,18] yet the underlying origin of this difference was not yet clearly addressed so far in the literature. As known, the materials in service are subject to changes in temperature, emerging from varying ambient conditions as well as from the generation of heat by the inner losses of the functional material.[19,20] The dependence of strain properties on temperature is therefore an issue of major concern for the design of actuators. It is thus of much significance to prepare a large-strain material showing a low hysteresis and a small temperature insensitivity for high-reliability actuators.

Rhombohedral BMT–PT compositions were reported to exhibit an obvious diffuse phase transition in the absence of any frequency dispersion, and were characterized by polar domains of ~50 nm with a frozen-in polarization (static) state, which can only be switched under a sufficiently strong electric field.[13] Recent investigations demonstrated that the addition of an appropriate amount of PZ could facilitate the domain switching by means of a change in the dynamics of the polar nanoregions (PNRs) from a static state to a dynamic state.[9,15] By comparison, PMN was generally considered as a canonical relaxor material at room temperature with randomly distributed PNRs of ~1.5 nm.[11,21,22] On cooling, their dynamics slows down enormously and at a low enough temperature, i.e., freezing temperature (T_f, ~−53 °C), the PNRs become frozen into a nonergodic state.[23–25] For their solid solutions with PT, the addition of PT tends to retard the dynamics of PNRs in PMN, such that 0.7PMN–0.3PT becomes a nonergodic relaxor at room temperature, but still has a relatively smaller domain size than 0.7BMT–0.3PT.[26]

In this work we reported a new ternary system of $(0.7-x)$BMT–xPMN–0.3PT by means of their respective dielectric behavior and strain characteristics of two end binary compositions: 0.7BMT–0.3PT and 0.7PMN–0.3PT. On the one hand, the substitution of PMN for BMT was expected to produce a gradual change in the size and dynamics of the PNRs from a static state to a dynamic state for the 0.7BMT–0.3PT end composition. On the other hand, the replacement of BMT for PMN would enhance the relaxor degree of the 0.7PMN–0.3PT end composition owing to the increased compositional inhomogeneities. The selected composition points were drawn as red dots in a phase diagram as shown in Fig. 1, in which the blue dashed line stands for the approximate position of the classical morphotropic phase boundary (MPB) for the BMT–PMN–PT ternary system. The inter-substitution of PMN and BMT was found to generate a large-strain platform in a wide composition range. A temperature-insensitive large strain (~0.3% in average at 5 kV/mm) was successfully obtained in the $x = 0.2$ sample. In situ synchrotron X-ray diffraction was applied to explore the mechanism and hysteresis behavior of generating large strains in different compositions and to identify the response of the structural evolution to the external electric field. The thermal stability of the electric field induced strains was specially discussed in combination with the composition–temperature–structure phase diagram, ferroelectric polarization/strain loops and polarization current density curves.

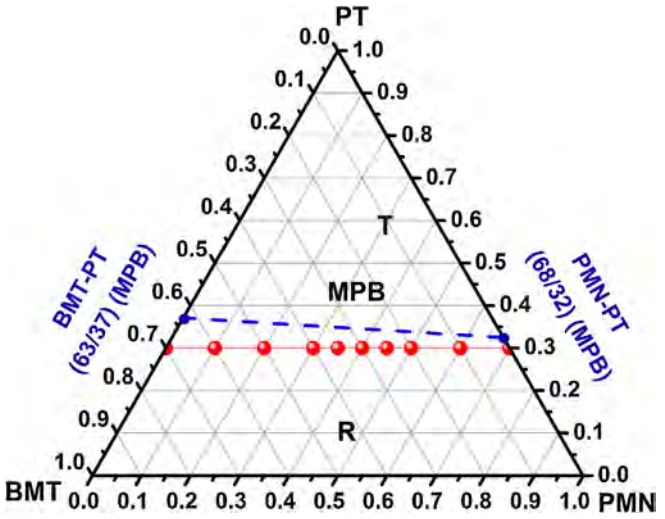

Fig. 1. Schematic phase diagram of $(0.7-x)$BMT–xPMN–0.3PT ternary system.

2. Experimental

The $(0.7-x)$BMT–xPMN–0.3PT ceramics in the range from $x = 0.0$–0.7 (Fig. 1) near the MPB of the BMT–PT–PMN ternary system were synthesized by a conventional solid-state reaction method using high-purity Bi_2O_3 (≥99.5%), Nb_2O_5 (≥99%), PbO (≥99%), $(MgCO_3)_4{\cdot}Mg(OH)_2{\cdot}5H_2O$ (≥99%) (Sinopharm Chemical Reagent Co. Ltd, Shanghai, China) and TiO_2 (purity ≥99%, Xilong Chemicals, Guangdong, China) as raw materials. After weighing according to the stoichiometric formula, the powders were ball-milled with ethanol and zirconia media for 6 h. The dried powders were calcined twice at 850 °C for 2 h and then ball milled again for 8 h. The powders were uniaxially pressed into pellets with 10 mm in diameter and the pellets were sintered in sealed crucibles at 1030–1200 °C for 2 h. For electrical measurements, the silver paste was painted on major sides of the samples and fired at 550 °C for 30 min.

The relative densities were evaluated by the Archimedes method. The crystal structure of the as-synthesized powders was examined by conventional X-ray diffraction with a step size of 0.02° at a speed of 4 °/min (XRD, D/Max-RB, Rigaku, Japan) and high-resolution synchrotron X-ray diffraction with a step size of 0.01° and a count time of 0.5 s. Morphological investigation was carried out by using a scanning electron microscope (SEM, JEOL JSM-6490LV, Tokyo, Japan). Before the SEM observation, the samples were polished and thermally etched at ~950 °C for 30 min. Dielectric properties of unpoled and poled samples were measured as a function of temperature and frequency by an LCR meter (Agilent E4980A, Santa Clara, CA). Polarization and strain versus electric field (P–E and S–E) hysteresis curves were measured at a frequency of

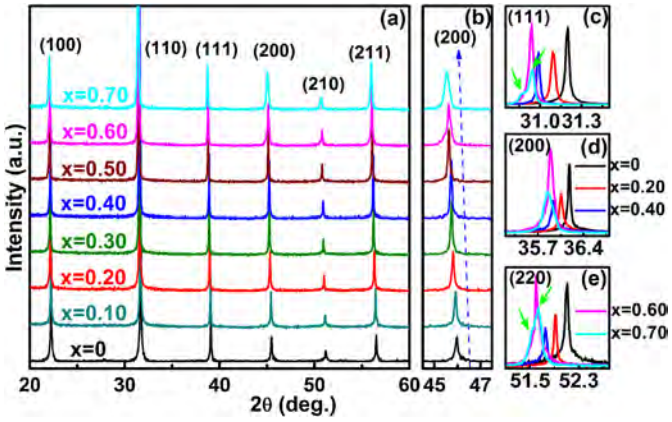

Fig. 2. (a) Room-temperature conventional XRD patterns and (b) locally magnified (200) diffraction lines of $(0.7-x)$BMT–xPMN–0.3PT ceramics as indicated, and synchrotron XRD patterns on (c) (1 1 1), (d) (2 0 0) and (e) (2 2 0) reflections for samples as indicated.

1 Hz as a function of composition and temperature under bipolar and unipolar fields using a ferroelectric measuring system (Precision multiferroelectric, Radiant Technologies Inc., Albuquerque, NM) connected with an accessory laser interferometer vibrometer (SP-S 120E, SIOS Meβtechnik, GmbH, Ilmenau, Germany). The polarization current density versus electric field (J–E) curves were simultaneously collected. For in situ synchrotron X-ray diffraction measurement, thin gold electrodes were sputtered onto two well-polished sides of the ceramic disks. All the synchrotron X-ray diffraction measurements were taken at Shanghai Synchrotron Radiation Facility (SSRF) using beam line 14B1 ($\lambda = 1.2378$ Å).

3. Results

3.1. Compositional dependence of the crystal structure and microstructure

Fig. 2(a and b) shows the phase structural change of $(0.7-x)$BMT–xPMN–0.3PT solid solution ceramics. It is obvious that all studied compositions demonstrate a single perovskite structure in terms of typical diffraction patterns. It seems that no splitting was observed in all diffraction peaks through a conventional XRD technique. Considering that the difference between the pseudocubic symmetry and the rhombohedral symmetry with a slight small distortion is very small, the synchrotron powder XRD patterns of (1 1 1), (2 0 0), and (2 2 0) reflections were recorded for a few selected compositions, as shown in Fig. 2(c–e). An obvious splitting of the (1 1 1) and (2 2 0) diffraction lines in addition to a single (2 0 0) line was observed for the 0.7PMN–0.3PT ceramic, as denoted by green arrows, meaning that the average symmetry of the $x = 0.7$ sample is rhombohedral. As $x = 0.6$, the sample's phase structure has already changed into a pseudocubic symmetry, as evidenced by the single peak of (1 1 1), (2 0 0), and (2 2 0) diffraction lines. This illustrates that the distortion of 0.7PMN–0.3PT is so small that the substitution of a small amount of BMT for PMN can reduce its distortion and thus result in the presence of a pseudocubic symmetry. With further increasing the BMT content, the samples maintain the pseudocubic structure till the 0.7BMT–0.3PT sample ($x = 0$), as found in BMT–PT binary system with low PT contents.[14] Nevertheless, the locally magnified (2 0 0) diffraction peaks in Fig. 2(b) reveal a shift of the diffraction peaks to higher diffraction angles with increasing the BMT content, indicating that there is a slight lattice shrinkage. This is probably due to relatively large ionic radii of Pb^{2+} and Nb^{5+} compared to those of Bi^{3+} and Ti^{4+} at the A- and B-sites ($CN = 12$, $R_{Pb} = 1.49$ Å, $R_{Bi} = 1.45$ Å; $CN = 6$, $R_{Nb} = 0.64$ Å, $R_{Ti} = 0.605$ Å), respectively.[27] For the same reason, the lattice distortion of this ternary system was slightly decreased from the 0.7PMN–0.3PT ceramic to the 0.7BMT–0.3PT ceramic.

The microstructure of the selected compositions is shown in Fig. 3. It is obvious that the introduction of PMN has a strong influence on the evolution of the microstructure. Pure BMT–PT ($x = 0$) shows small grains and a relatively low density (~94%), which keeps consistency with the reference report.[13] With the introduction of PMN, the grain size increased significantly. The average grain size, as determined with a linear interception method, increased from ~0.85 μm for 0.7BMT–0.3PT sample ($x = 0$) to ~2.2 μm, ~2.6 μm and ~3.5 μm for the $x = 0.2$, 0.35 and 0.45 samples, respectively. Compared with the $x = 0$ sample, the relative density obviously increased with increasing the PMN content (>97%). This result indicates that the addition of PMN tends to modify the sintering of BMT–PT but simultaneously promote its grain growth.

3.2. Evolution of dielectric relaxor behavior in $(0.7-x)$BMT–xPMN–0.3PT

The dielectric permittivity (ε) and loss tangent ($\tan\delta$) of $(0.7-x)$BMT–xPMN–0.3PT ceramics were plotted as a function of temperature and frequency, as shown in Fig. 4(a and b) and (c and d). It can be seen that the frequency dependence of the dielectric permittivity first gradually increases and then decreases after a maximum at $x = 0.4$ with increasing the PMN content. It seems that the exchange of PMN and BMT in $(0.7-x)$BMT–xPMN–0.3PT ternary system tends to enhance the relaxation degree of both end binary systems. The same information can be also obtained in frequency-dependent loss tangent versus temperature curves. The relaxor behavior is generally characterized by the diffuseness degree (γ), which can be calculated from a modified Curie–Weiss law,[28] and another parameter ΔT_{relax}, which is defined as the difference between two T_m values measured at 1 kHz and 1 MHz,[29] respectively. Obviously, both parameters reach the maximum at $x = 0.4$ (see Fig. 4e), suggesting that the $x = 0.4$ sample owns the strongest relaxor characteristics. For end binary systems, the 0.7BMT–0.3PT ceramic was reported to own a typical diffuse phase transition (DPT) behavior at the temperature for the dielectric maxima (T_m) in the absence of the frequency dispersion,[13] which was usually considered as an intermediate state between normal ferroelectrics and relaxor ferroelectrics.[30] By comparison, only a weak relaxor behavior around T_m was observed in 0.7PMN–0.3PT.[31] The disordered distribution of different ions at one or more equivalent crystallographic sites would cause the

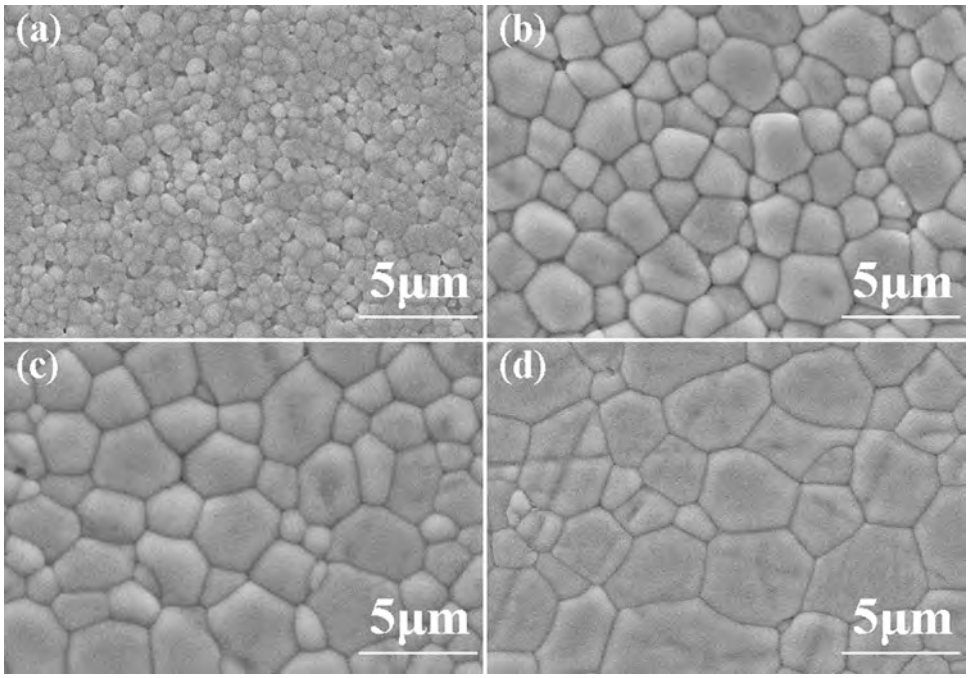

Fig. 3. SEM micrographs of $(0.7-x)$BMT–xPMN–0.3PT ceramics sintered at their optimum temperatures: (a) $x=0.0$, (b) $x=0.2$, (c) $x=0.35$ and (d) $x=0.45$.

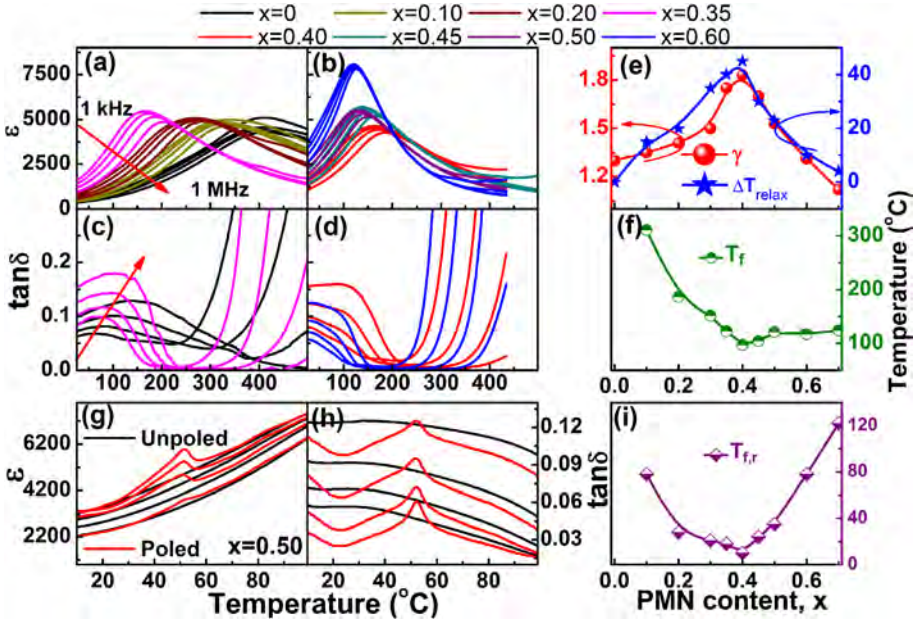

Fig. 4. Dielectric permittivity (a) and (b) and loss tangent (c) and (d) as a function of temperature and frequency for unpoled $(0.7-x)$BMT–xPMN–0.3PT ceramics as indicated; (e) the ΔT_{relax} and γ values, and (f) the T_f values with varying the PMN content; the comparison of the dielectric permittivity (g) and loss tangent (h) for the $x=0.5$ sample before and after poling; (i) the $T_{f,r}$ value as a function of the PMN content.

formation of random local fields, which are responsible for the growth of PNRs.[9,19,32] The size and dynamics of these PNRs and correlations among them are closely associated with the evolution of relaxor behavior.[33] The coexistence of PMN and BMT in $(0.7-x)$BMT–xPMN–0.3PT ternary system tends to enhance the random local fields of the two end compositions, resulting in a gradual increase of the dynamics of PNRs as well as a decrease in size of PNRs. A freezing temperature, T_f, which was usually defined as the onset temperature of the emergence of nonergodic PNRs from the ergodic matrix on cooling, can be obtained by fitting the measured dielectric permittivity versus temperature curves at different frequencies for unpoled samples (Fig. 4(a and b)) to the Vogel–Fulcher relationship,[34] as shown in Fig. 4(f). It changes fast with increasing the PMN content at BMT-rich side and then slowly at PMN-rich side. The minimum T_f value was obtained in the $x=0.4$ sample, which is consistent with the fact that this sample owns the strongest dielectric relaxation behavior among the studied compositions.

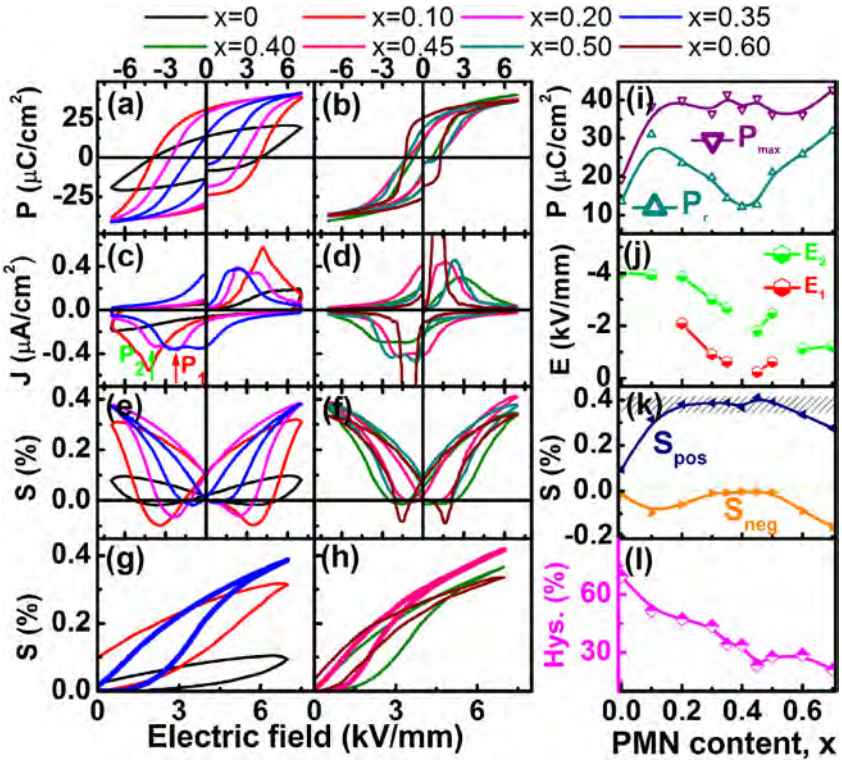

Fig. 5. Polarization versus electric field loops (a) and (b), the corresponding polarization currents (c) and (d), bipolar strain loops (e) and (f) and unipolar strain loops (g) and (h) for samples with different x values as indicated; (i) polarization values (P_r and P_{max}), (j) the electric field values E_1 and E_2 at polarization current peaks P_1 and P_2, (k) both the positive strain (S_{pos}) and negative strain (S_{neg}) and (l) the hysteresis degree shown as a function of the PMN content.

Moreover, it should be noted that no spontaneous relaxor to ferroelectric phase transition was observed below T_m for all unpoled samples,[23,35–37] indicating that these compositions are canonical relaxors. However, an external electric field is strong enough to overcome the random fields and induce a macroscopically detectable ferroelectric order.[38] The induced ferroelectric order can be either unstable or stable upon removal of the applied electric field, depending on whether it is an ergodic state or nonergodic state at room temperature.[39] The transition temperature ($T_{f,r}$) from the electric field induced ferroelectric order to relaxor state can be clearly grasped in the dielectric permittivity and loss tangent versus temperature curves of poled samples upon heating, using the $x = 0.5$ poled ceramic as an example shown in Fig. 4(g and h), in which the temperature at the dielectric anomalies is denoted as $T_{f,r}$. The $T_{f,r}$ values determined as above was shown as a function of the PMN content in Fig. 4(i). This temperature can be approximately regarded as the end temperature of the transformation of ergodic phases to nonergodic phases on cooling or the starting temperature of ergodic states appearing from nonergodic states on heating. It changes slowly with increasing the PMN content at BMT-rich side and then fast at PMN-rich side.

3.3. Compositional dependence of the large electrostrain in (0.7 − x)BMT–xPMN–0.3PT

P–E hysteresis loops of $(0.7 - x)$BMT–xPMN–0.3PT ceramics are shown in Fig. 5(a and b) and the corresponding J–E curves were simultaneously collected as they are more sensitive to the polarization state (Fig. 5(c and d)). The 0.7BMT–0.3PT ceramic shows an unsaturated P–E loop probably because this composition usually has relatively high dielectric losses.[40] After a small amount of PMN ($x = 0.1$) is added, a well-saturated P–E loop is observed owing to the improved sinterability (Fig. 3). Meanwhile, the corresponding J–E curve shows an obvious current peak, indicating a significant improvement of the ferroelectricity probably gained from an activation of the frozen domains, in addition to the effect of the decreased leakage current. Moreover, a further addition of PMN is found to make P–E loops slimmer and slimmer as $x < 0.4$. On the contrary, as $x > 0.4$, the substitution of PMN for BMT is found to make P–E loops become more and more square. The $x = 0.4$ composition behaves like a typical relaxor since its P–E loop is very slim and its dielectric permittivity is most strongly dependent on measuring frequency in all studied samples. Moreover, the change of ferroelectricity can be also clearly reflected by the remanent polarization (P_r) of different compositions, as seen from Fig. 5(i). It can be seen that the P_r value reaches the minimum at $x = 0.4$. Although a long-range ferroelectric state can be induced by an electric field in all samples, yet it becomes more unstable as the relaxor degree of the sample increases due to an increase of the random local field. Nevertheless, the maximum polarization (P_{max}) value does not change much for different compositions because it is mainly related to the poling state of the electric field induced long-range ferroelectric phases.[41]

The J–E curves for $(0.7 - x)$BMT–xPMN–0.3PT ceramics exhibit two obviously segregated current peaks (marked by P_1 and P_2) in a wide composition range ($0.2 \le x \le 0.5$) evolving

from a single current peak for the $x < 0.2$ and $x > 0.5$ compositions, as shown in Fig. 5(c–d). The appearance of two broad current peaks is indicative of the coexistence of nonergodicity and ergodicity in these samples.[9,42] The electric field induced ferroelectric ordering after the first cycle would revert back to its initial ergodic state as the applied field is released, generating the first polarization current peak P_1. By comparison, the appearance of the second polarization current peak P_2 is due to the back-switching of field induced ferroelectric states from initial nonergodic states. The field values E_1 and E_2 corresponding to the current peaks P_1 and P_2, respectively, were shown in Fig. 5(j). As the relaxor degree increases with the variation of x, E_2 tends to decrease owing to the decrease in the size of PNRs. However, the hysteresis effect of the induced ferroelectric back to ergodic relaxor phase transition is responsible for the fact the E_1 value with a negative sign is getting close to zero, and even becomes positive in some cases (P_1 appears in the fourth quadrant), depending on the dynamics of the involved ergodic PNRs.[42] Only a single current peak observed in both BMT-rich and PMN-rich compositions ($x \leq 0.1$ or $x \geq 0.6$) should be ascribed to the domain switching, indicating that these compositions would be dominantly composed of nonergodic relaxor phases. A polarization current platform instead of any obvious peak was observed for the $x = 0.4$ sample, meaning that this sample is dominated by ergodic phases at room temperature.

A change from typical butterfly loops to sprout loops with the substitution of PMN for BMT (Fig. 5(e and f)) indicates the similar variation of ferroelectricity and dielectric behavior as mentioned in Fig. 5(a and b) and Fig. 4(a–d), respectively. The negative strain (S_{neg}) value generally decreases and approaches to nearly zero in the composition range of $0.2 < x \leq 0.5$ where a strain platform (positive strain, $S_{pos} \sim 0.4\%$) is obtained, as shown in Fig. 5(k). The coexistence of nonergodic and ergodic states within a wide composition range would provide a structural base for the composition insensitivity of large electrostrains. Nevertheless, two strain maxima lying at BMT-rich side and PMN-rich side (e.g. ~0.38% at $x = 0.35$ and ~0.42% at $x = 0.45$ under 7 kV/mm) can be distinguished within the phase coexistence zone, as shown in Fig. 5(g and h). The electric field induced large strain was generally ascribed to reversible ergodic phase-ferroelectric phase transformation,[43,44] which usually appears close to the phase boundary (or phase coexistence zone) of ergodicity and nonergodicity. As a result, the formation of two strain maxima in this study should be attributed to the composition modified room-temperature phase structural evolution from nonergidic phases to ergodic phases and then to nonergodic phase, as shown in Fig. 4. Moreover, the maximum unipolar strains with increasing fields exhibit an *S*-shape curve but own different values under the same field amplitude, indicating a different evolution process of the domain in response to the electric field. For the $x = 0.35$ sample, no obvious strain value can be observed until the electric field reaches 1 kV/mm. As the electric field increases above 1 kV/mm, the strain value gradually increases. The increase of the strain between 1 kV/mm and 2 kV/mm would originate from the reorientation of ergodic PNRs. A fast increase of strains occurs as the field is above 2.5 kV/mm. As for the $x = 0.45$ sample, a small strain value can be observed even below 1 kV/mm. An obvious increase of strains seems to start from 1.5 kV/mm. By comparison, the $x = 0.45$ sample owns a relatively low driving electric field. Moreover, the generated strains of the $x = 0.45$ sample under the same fields are generally larger than those of the $x = 0.35$ sample. Nevertheless, the mechanisms for generating large strains still need more direct and stronger experimental supports from phase structural variations.

The strain hysteresis, which is related to the piezoelectric loss, can be obtained from the ratio of the widest part of the unipolar *S–E* loop over the maximum strain level (Hys. = W_{max}/S_{max}), as shown in Fig. 5(l). It is obvious that a large strain hysteresis was observed for the pure BMT–PT ceramic owing to the existence of the large and static domain with a slow response to the external field. With increasing the PMN content, an obvious decrease of the strain hysteresis together with an enhancement of the strain value was observed. As stated, the addition of PMN can turn the static domains into the nonergodic state, resulting in an increased mobility of domains. Generally, the strain hysteresis of BMT-rich compositions is larger than that of PMN-rich compositions because the switching kinetics of domains for BMT-rich compositions is relatively sluggish at room temperature as a result of bigger domain sizes. In large-strain-generating compositions, the increased hysteresis should be mainly ascribed to the field induced structural phase transition from ergodic phase to a long-range ferroelectric phase, as compared to traditional Pb-based soft piezoceramics whose strain hysteresis mainly originates from the ferroelectric domain reorientation. It is worthy of note that the $x = 0.45$ sample owns a much lower hysteresis than the $x = 0.35$ sample although both of them own the maximum strains in their respective compositional ranges. In addition to the domain size, the structural mechanism during phase transition will be discussed infra by means of in situ synchrotron X-ray diffraction measurement. The $x = 0.4$ sample does not exhibit the smallest hysteresis although it is dominated by an ergodic state. This should be ascribed to the fact that the S_{max} value of the $x = 0.4$ sample is relatively small compared to that of the $x = 0.45$ sample although their W_{max} values in its unipolar strain loop are nearly equal. The lowest strain hysteresis (~23%) was observed in the $x = 0.45$ sample, which is much smaller than that reported in other widely studied bismuth-based perovskite materials (mostly exceeding 60%); however, their achieved maximum strains are comparable.

3.4. Thermal stability of electrostrains in $(0.7-x)$BMT–xPMN–0.3PT

The temperature dependence of the strains should be a key feature for actuator systems since the strain fluctuation would degrade the positioning accuracy. Considering the effect of the leakage current at high temperatures, unipolar strains with temperature were measured under a relatively low driving field (5 kV/mm). An exciting result to be noted in this study rests with the temperature insensitive strain behavior of the currently studied composition with $x = 0.2$, as provided in Fig. 6(a). This behavior was observed from room temperature up to 180 °C. It can be seen that the unipolar strain retains its room-temperature

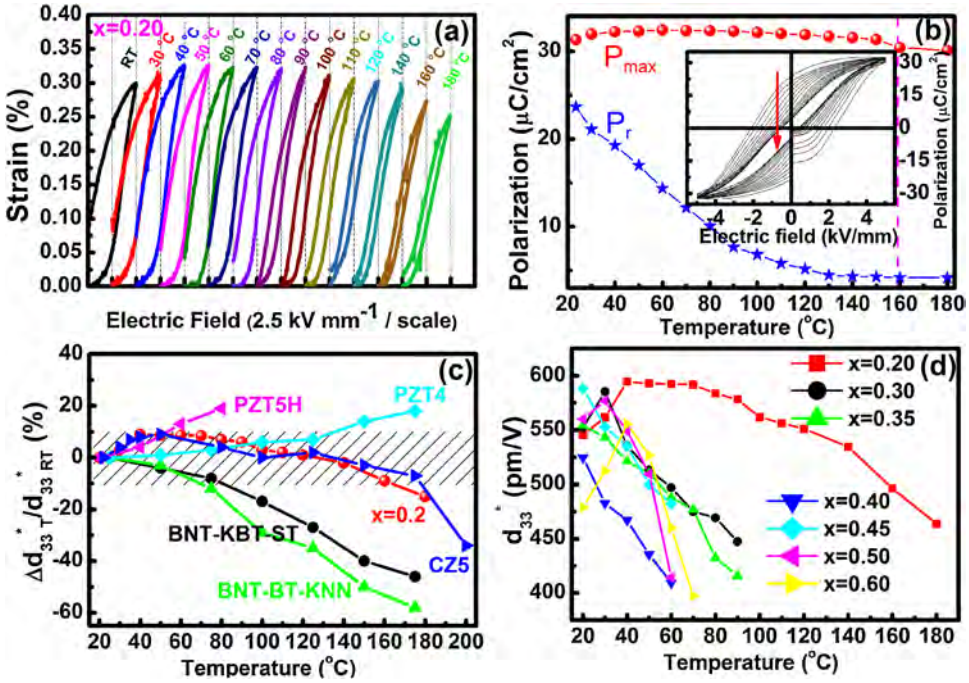

Fig. 6. (a) Temperature dependence of the unipolar strain at 5 kV/mm for the $x = 0.2$ sample, (b) the variation of P_r and P_{max} values as a function of temperature for the $x = 0.2$ sample; the inset of (b) shows the corresponding temperature-dependent P–E loops, (c) the variation of normalized strains $d_{33}{}^{*}{}_{T}$ against temperature for various ferroelectric ceramics relative to their room temperature values $d_{33}{}^{*}{}_{RT}$ and (d) the normalized strain $d_{33}{}^{*}$ changing with temperature for different samples as indicated.

value of 0.3% at 5 kV/mm (S_{max}/E_{max} = ~600 pm/V) up to a temperature as high as 160 °C. The variation of such a large strain value is kept within ±10% of its room-temperature value within a wide working temperature range, suggesting promising potential for actuator applications. In addition, the P_{max} and P_r values of the $x = 0.2$ sample behave differently with increasing temperature, as shown in Fig. 6(b). The value of P_{max} does not change much in the temperature range from room temperature to 160 °C and becomes obviously small as the temperature gets close to its T_f value (180 °C) as indicated in Fig. 4(f). However, as the temperature cools below its T_f value, the P_r values only increase slowly instead of abruptly increasing as noted in BNT-based perovskite systems.[45] These results hint that the appearance of nonergodic phases from ergodic phase is a gradual process in the $x = 0.2$ sample. From the energy point of view, this kind of phase coexistence in a wider temperature range allows the ergodic phase to be electrically driven into a long-range ferroelectric ordering, resulting in an equivalent P_{max} value from room temperature up to its T_f value.

A comparison of the relative variation of strains with temperature of the $x = 0.2$ sample with some widely studied systems in terms of normalized strain $d_{33}{}^{*}$ (=S_{max}/E_{max}) is provided in Fig. 6(c) (the data for PZT5H,[46] PZT4,[47] BNT–BT–KNN[18] and BNT–KBT–ST[10] were taken from figures in the respective references). The LF4T textured ceramic was reported by Saito et al.[47] to show good strain characteristics. However, it is not compared in this study since it requires an extremely complex texturing technology. It is noted that the thermal stability of the electric field induced strains of the current composition is much better than some Pb-based piezoelectric ceramics such as PZT5H and PZT4, and also superior to BNT-based relaxor ferroelectrics.[10,18] Although its temperature stability of strains is comparable to that of the recently reported KNN-based system CZ5,[48] yet the current composition shows nearly two times larger normalized strains $d_{33}{}^{*}$ than the CZ5 ceramics (0.13% at 4 kV/mm, $d_{33}{}^{*}$ = 325 pm/V for CZ5, and 0.30% at 5 kV/mm, $d_{33}{}^{*}$ = 600 pm/V for the current composition). The strain characteristic indicates that the studied material has promising applications requiring the temperature-stable outputs as well as the large output signal. Moreover, the result of superior temperature-insensitivity was also brought into the compositional context by comparing the studied samples with different PMN contents, as shown in Fig. 6(d). It is demonstrated that the $x = 0.2$ ceramic sample exhibits the optimum temperature-stable strain behavior. For samples lying at both ends of the ternary system (for examples, $x = 0.2$, 0.3 and $x = 0.5$, $x = 0.6$), it can be seen that there are wide strain peaks with changing temperature. However, the strain behavior of the compositions in the middle of the ternary system such as $x = 0.35$, 0.4 and 0.45 experiences a monotonous decrease with increasing the measuring temperature. These results reveal that the initial state (ergodicity or nonergodicity) of the composition at room temperature would be closely associated with the variation of strains with increasing temperature. The sample with the best thermal stability of strains appears in BMT-rich compositions ($x = 0.2$), instead of PMN-rich compositions, indicating that the thermal stability of electrostrains should be also related to the specific domain state of the composition. It can be believed that PNRs of different sizes and dynamics would exhibit different stabilities against temperature or compositional variation.

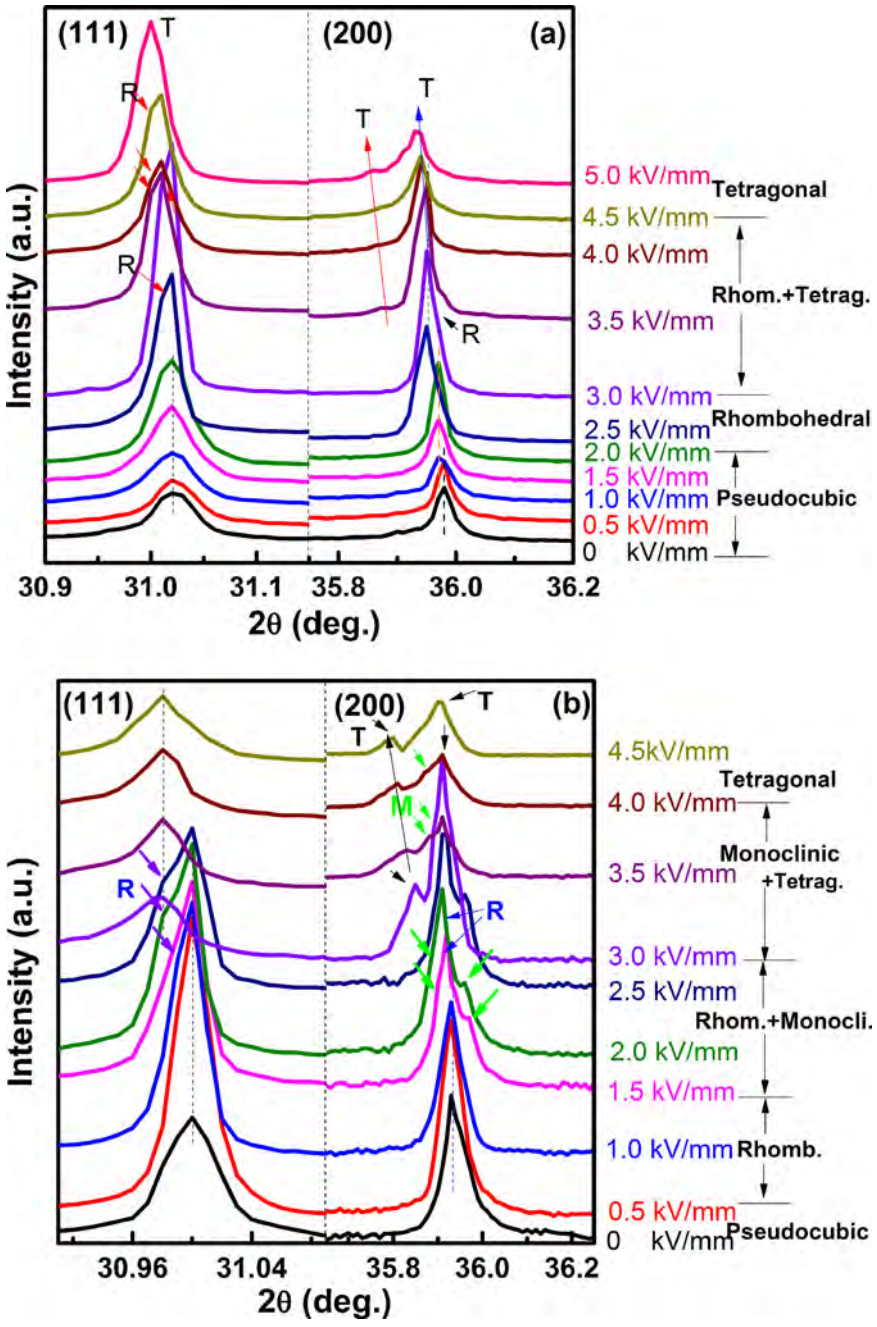

Fig. 7. Evolution of (1 1 1) and (2 0 0) diffraction lines for the (a) $x = 0.35$ and (b) $x = 0.45$ samples under different external electric fields.

4. Discussion

Considering that the application of electric fields can induce phase transformation or domain switching (PNR reorientation) and further lead to the change of the position and intensity of diffraction lines, the in situ high-resolution synchrotron X-ray diffraction was used to detect these changes under electric fields of various magnitudes with a step of 0.5 kV/mm, as shown in Fig. 7.

As for the $x = 0.35$ sample, no obvious change can observed from typical (1 1 1) and (2 0 0) diffraction lines until the field reaches 1 kV/mm (Fig. 7(a)) because the electric field amplitude is not high enough to induce any change of the domains, compared with the random field of PNRs. A significant increase of the peak intensity with no obvious peak shift is then observed with further increasing the field to 2 kV/mm. This change can be ascribed to the polarization alignment of PNRs along the electric field direction as the random field is overcome. Simultaneously the phase structure of the sample during this period should still keep pseudocubic symmetry as evidenced by the single (1 1 1) and (2 0 0) peaks. As the applied field continues to rise ($2.5\ \text{kV/mm} \leq E \leq 3.0\ \text{kV/mm}$), it can be seen that the (2 0 0) diffraction peak remains single and obviously shifts toward the lower-angle side, together with a continuous increase of the peak intensity. However, the (1 1 1) peak tends to become asymmetric with a shoulder appearing at the lower angle side as denoted by

some red arrows. Therefore, the phase structure of the sample can be assigned to rhombohedral instead of an initial pseudocubic, meaning that the initially existing PNRs start to become a short-range ordered polar phase. The applied electric field tends to make the unit cell become more distorted. Further increasing the electric field would induce an additional peak at the lower-angle side of the (2 0 0) peak, which gradually shifts away from the initial (2 0 0) peak. At the same time, the low-angle shoulder of the (1 1 1) peak is maintained in a certain field range and then gradually merges into a single (1 1 1) peak as the electric field reaches 5 kV/mm. These changes suggest that a tetragonal phase with a long-range ferroelectric ordering starts to appear after an electric field of 3 kV/mm and become nearly pure after 5 kV/mm. That is to say, the rhombohedral and tetragonal phases coexist in the field range of 3–5 kV/mm.

For the $x = 0.45$ sample (Fig. 7(b)), the (2 0 0) diffraction peak at zero field is asymmetric at zero field probably as a result of the diffuse scattering induced by the existence of PNRs.[49] A pseudocubic symmetry can be illustrated by a single (1 1 1) peak. An obvious increase of the (1 1 1) peak intensity occurs as soon as the field reaches only 0.5 kV/mm, indicating an easier alignment of PNRs in the $x = 0.45$ sample than in the $x = 0.35$ sample. With increasing the field to 1 kV/mm, a single (2 0 0) peak is kept while the (1 1 1) peak starts to become asymmetry and a slight shoulder can be observed at the lower angle side of the (1 1 1) peak. It means that a pseudocubic matrix composition with randomly distributed PNRs starts to transform into a rhombohedral phase with a short-range ordered polar phase through a lattice distortion. With further increasing the electric field from 1 kV/mm to 2.5 kV/mm, an obvious profile shape change of the (2 0 0) peak is observed. The single (2 0 0) peak is split into three distinct peaks with two shoulders at both lower and higher angle sides (denoted by green arrows) of the rhombohedral (2 0 0) peak (denoted by blue arrows). At the same time, the splitting of the (1 1 1) peak can also be obviously observed. This is similar to that observed in Pb-based perovskite systems where the structure was classified as a coexistence of rhombohedral and monoclinic phases.[50] When the field approaches to 3 kV/mm, three (2 0 0) peaks can be still observed but exhibit a reduced peak intensity and the splitting degree of the (1 1 1) peak also decreases. As the electric field is further increased up to 4.5 kV/mm, a tetragonal symmetry with a long-range ferroelectric ordering becomes more and more evident, as evidenced by two clearly separated $(0\,0\,2)_T$ and $(2\,0\,0)_T$ peaks and a single (1 1 1) peak.

Although the $x = 0.35$ sample at BMT-rich side and the $x = 0.45$ sample at PMN-rich side exhibit similar crystal structural variation process in response to external electric fields, yet some differences have been still detected as seen from Fig. 7. Generally, it can be believed that the orientation and growth of ergodic PNRs and then transformation into a long-range ferroelectric ordering, and the accompanying crystal structural transition should be responsible for the formation of large electrostrains in this system. The coexistence of ergodic and nonergodic phases should be a pre-requisite condition for the generation of large strains, which provides a minimum energy barrier between the ergodic relaxor state and the long-range ferroelectric state. However, this energy barrier is still not ignorable, such that the forward and backward phase transition exhibits hysteresis (Fig. 5(g and h)). Compared with the $x = 0.35$ composition, more intermediate phases of different symmetries participating in the response process of PNRs to the electric field can reduce the required activation field because of a reduced energy barrier between neighboring steps, being basic reasons why the $x = 0.45$ sample can own a relatively large electrostrain value and a relatively small hysteresis (see Fig. 5(k and l)). For simplicity, the in situ synchrotron X-ray diffraction analysis was not carried out for other samples which might be composed of a certain amount of nonergodic phases. Although the existence of nonergodic phases should more or less contribute to the variation of diffraction lines under different fields, yet the strain hysteresis of these samples should be little affected by an irreversible phase transition of nonergodic phase to a long-range ferroelectric phase.

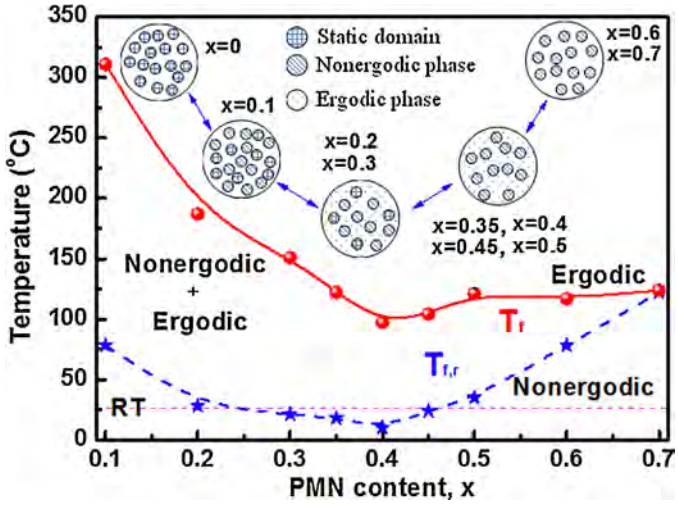

Fig. 8. The phase diagram of $(0.7 - x)$BMT–xPMN–0.3PT ternary system, in which three phase zones as indicated have been separated by the broken blue line ($T_{f,r}$ values) and the solid red line (T_f values). The insets schematically show the room-temperature domain structures for different compositions.

In order to clarify the reason why the $x = 0.20$ sample has better thermal stability of the strain than other compositions of the studied ternary system, the phase diagram of $(0.7 - x)$BMT–xPMN–0.3PT ceramics was plotted as a function of composition by using both T_f and $T_{f,r}$ values, as shown in Fig. 8. According to the definitions of both critical temperatures as mentioned above, three phase zones can be generally distinguished. It can be found that the samples are composed of coexisted ergodic and nonergodic phases in a wide temperature, particularly for the $x = 0.2$ sample. This should be a solid foundation for the achievement of excellent thermal stability of electrostrains because the coexistence of ergodicity and nonergodicity was believed to the structural base for forming large electrostrains. By comparison, the difference between T_f and $T_{f,r}$ values is particularly small in BNT-based large-strain-generating systems[10,45] and PMN, PLZT canonical relaxors.[51,52] In addition, the T_f of the studied compositions owns a relatively high value, which may also help to improve

the thermal stability of strains because the pure ergodic phase zone can appear at a higher temperature.

As reported, pure 0.7BMT–0.3PT ceramics own large static domains.[13] The substitution of a small amount of PMN tends to gradually decrease the size and volume of the static domains and then nonergodic relaxor phases start to appear at $x = 0.1$. Further increasing the PMN content results in a continuous decrease of the static domains, and simultaneously part of nonergodic phases transform into ergodic phases. It is then possible that the initially static domains, nonergodic and ergodic PNRs coexist in the $x = 0.2$ composition at room temperature, as schematically illustrated in the inset of Fig. 8. For the same reason, the existence of static domains of large sizes at room temperature would allow the transformation from nonergodic phases to ergodic phases to last in a relatively broad temperature range during heating, thus generating temperature-insensitive large strains. As the static domain structure disappears from the samples owing to the increase of the PMN content, the temperature range for the transition from nonergodic phases to ergodic phases or vice versa becomes narrower and narrower (Fig. 8). It can be believed that different domain structures (PNR size or dynamics) and phase structural evolution processes would respectively contribute to the difference in both the temperature dependence and the hysteresis degree of electrostrains between BMT-rich and PMN-rich ternary compositions.

5. Conclusions

$(0.7 - x)$BMT–xPMN–0.3PT ($x = 0$–0.7) ferroelectric ceramics were investigated in terms of their phase structure, dielectric behavior and ferroelectric polarization/strain characterizations. The inter-substitution of PMN and BMT was found to induce an obvious evolution of the dielectric relaxor behavior from two end members of a diffuse-type BMT–PT binary system and a weak relaxor PMN–PT binary system, during which a large-strain platform within a wide composition range was observed. In situ high-resolution synchrotron X-ray diffraction measurements further suggest that the mechanism for generating large strains should be ascribed to the electric field induced relaxor to ferroelectric phase transformation that also involves a crystallographic symmetry change. More intermediate phases induced by external fields make PMN-rich compositions to own smaller strain hysteresis than BMT-rich compositions owing to reduced energy barriers. Most interestingly, the $x = 0.2$ sample exhibits field-induced large strains of∼0.3% at 5 kV/mm (normalized strains $d_{33}^{*} = 600$ pm/V) varying less than 10% from room temperature up to 160 °C, showing great potentials for large-displacement actuator applications. The temperature insensitivity of electrostrains was mainly attributed to its special domain structure typical for BMT-rich compositions, which might allow two kinds of relaxor states to coexist in a broad temperature range. These findings provide a new approach toward an appropriate compositional design for low-hysteresis and temperature-insensitive large electrostrains in BMT-based relaxor ferroelectrics.

Acknowledgments

The authors would like to thank Shanghai Synchrotron Radiation Source for use of the synchrotron radiation facilities. Financial support from the National Natural Science Foundation of China (Grant No. 51272060) and an opening fund of State Key Laboratory of New Ceramic and Fine Processing at Tsinghua University is gratefully acknowledged.

References

1. Uchino K. *Piezoelectric actuators and ultrasonic motors*. Boston: Kluwer Academic Publishers; 1996.
2. Jaffe B, Cook WR, Jaffe H. *Piezoelectric ceramics*. New York: Academic Press; 1971.
3. Cross LE. Domain and phase change contributions to response in high strain piezoelectric actuators. *AIP Conf Proc* 2000;**535**:1–15.
4. Wang YU. Field-induced inter-ferroelectric phase transformations and domain mechanisms in high-strain piezoelectric materials: insights from phase field modeling and simulation. *J Mater Sci* 2009;**44**:5225–34.
5. Fu J, Zuo RZ, Wu SC, Jiang JZ, Li L, Yang TY, et al. Electric field induced intermediate phase and polarization rotation path in alkaline niobate based piezoceramics close to the rhombohedral and tetragonal phase boundary. *Appl Phys Lett* 2012;**100**:122902.
6. Tan X, Frederick J, Ma C, Aulbach E, Marsilius M, Hong W, et al. Electric-field-induced antiferroelectric to ferroelectric phase transition in mechanically confined $Pb_{0.99}Nb_{0.02}[(Zr_{0.57}Sn_{0.43})_{0.94}Ti_{0.06}]_{0.98}O_3$. *Phys Rev B* 2010;**81**:014103.
7. Zhang ST, Kounga AB, Aulbach E, Ehrenberg H, Rödel J. Giant strain in lead-free piezoceramics $Bi_{0.5}Na_{0.5}TiO_3$–$BaTiO_3$–$K_{0.5}Na_{0.5}NbO_3$ system. *Appl Phys Lett* 2007;**91**:112906.
8. Jarupoom P, Patterson E, Gibbons B, Rujijanagul G, Yimnirun R, Cann D. Lead-free ternary perovskite compounds with large electromechanical strains. *Appl Phys Lett* 2011;**99**:152901.
9. Fu J, Zuo RZ. Giant electrostrains accompanying the evolution of a relaxor behavior in Bi(Mg, Ti)O_3–$PbZrO_3$–$PbTiO_3$ ferroelectric ceramics. *Acta Mater* 2013;**61**:3687–94.
10. Wang K, Hussain A, Jo W, Rödel J. Temperature-dependent properties of $(Bi_{1/2}Na_{1/2})TiO_3$–$(Bi_{1/2}K_{1/2})TiO_3$–$SrTiO_3$ lead-free piezoceramics. *J Am Ceram Soc* 2012;**95**:2241–7.
11. Fu DS, Taniguchi H, Itoh M, Koshihara SY, Yamamoto N, Mori S. Relaxor $Pb(Mg_{1/3}Nb_{2/3})O_3$: a ferroelectric with multiple inhomogeneities. *Phys Rev Lett* 2009;**103**:207601.
12. Gupta SM, Li JF, Viehland D. Coexistence of relaxor and normal ferroelectric phases in morphotropic phase boundary compositions of lanthanum-modified lead zirconate titanate. *J Am Ceram Soc* 1998;**81**:557–64.
13. Randall CA, Eitel R, Jones B, Shrout TR, Woodward DI, Reaney IM. Investigation of a high T_c piezoelectric system: $(1 - x)$Bi$(Mg_{1/2}Ti_{1/2})O_3$–$(x)PbTiO_3$. *J Appl Phys* 2004;**95**:3633–9.
14. Suchomel MR, Davies PK. Predicting the position of the morphotropic phase boundary in high temperature $PbTiO_3$–$Bi(B'B'')O_3$ based dielectric ceramics. *J Appl Phys* 2004;**96**:4405–10.
15. Chen J, Li JY, Fan LL, Zou N, Ji PF, Liu LJ, et al. Enhanced piezoelectric and antiferroelectric properties of high-T_c perovskite of Zr-substituted $Bi(Mg_{1/2}Ti_{1/2})O_3$–$PbTiO_3$. *J Appl Phys* 2012;**112**:074101.
16. Fan LL, Chen J, Kang HJ, Liu LJ, Fang L, Deng JX, et al. Structure, piezoelectric, and ferroelectric properties of $BaZrO_3$ substituted $Bi(Mg_{1/2}Ti_{1/2})O_3$–$PbTiO_3$ perovskite. *J Appl Phys* 2012;**111**:104118.
17. Han HS, Jo W, Rödel J, Hong IK, Tai WP, Lee JS. Coexistence of ergodicity and nonergodicity in $LaFeO_3$-modified $Bi_{1/2}(Na_{0.7}8K_{0.22})_{1/2}TiO_3$ relaxors. *J Phys Condens Matter* 2012;**24**:365901.
18. Zhang ST, Kounga AB, Aulbach E, Jo W, Granzow T, Ehrenberg H, et al. Lead-free piezoceramics with giant strain in the system $Bi_{0.5}Na_{0.5}TiO_3$–$BaTiO_3$–$K_{0.5}Na_{0.5}NbO_3$ II. Temperature dependent properties. *J Appl Phys* 2008;**103**:034108.

19. Zheng JH, Takahashi S, Yoshikawa S, Uchino K, de Vries JWC. Heat generation in multilayer piezoelectric actuators. *J Am Ceram Soc* 1996;**79**:3193–8.
20. Kungl H, Hoffmann MJ. Method for the estimation of the total displacement of ferroelectric actuators under mixed thermal and electrical loading. *Sens Actuators A: Phys* 2008;**144**:328–36.
21. Cross LE. Relaxor ferroelectrics: an overview. *Ferroelectrics* 1994;**151**:305–20.
22. Xu GY, Shirane G, Copley JRD, Gehring PM. Neutron elastic diffuse scattering study of $Pb(Mg_{1/3}Nb_{2/3})O_3$. *Phys Rev B* 2004;**69**:064112.
23. Bokov AA, Ye ZG. Recent progress in relaxor ferroelectrics with perovskite structure. *J Mater Sci* 2006;**41**:31–52.
24. Grigalaitis R, Banys J, Brilingas A, Grigas J, Kania A, Slodczyk A. Dielectric dispersion in pure PMN and PMN with 10% PT single crystals. *Ferroelectrics* 2006;**339**:21–8.
25. Viehland D, Li JF, Jang SJ, Cross LE. Dipolar-glass model for lead magnesium niobate. *Phys Rev B* 1991;**43**:8316–20.
26. Bai FM, Li JF, Viehland D. Domain hierarchy in annealed (0 0 1)-oriented $Pb(Mg_{1/3}Nb_{2/3})O_3$–x%$PbTiO_3$ single crystals. *Appl Phys Lett* 2004;**85**:2313–5.
27. Shannon RD. Revised effective ionic radii and systematic studies of interatomie distances in halides and chaleogenides. *Acta Cryst* 1976;**A32**:751–67.
28. Uchino K, Nomura S. Critical exponents of the dielectric constants in diffused-phase-transition crystals. *Ferroelectr Lett* 1982;**44**:55–61.
29. Chen W, Yao X, Wei XY. Tunability and ferroelectric relaxor properties of bismuth strontium titanate ceramics. *Appl Phys Lett* 2007;**90**:182902.
30. Shvartsman VV, Kleemann W, Dec J, Xu ZK, Lu SG. Diffuse phase transition in $BaTi_{1-x}Sn_xO_3$ ceramics: an intermediate state between ferroelectric and relaxor behavior. *J Appl Phys* 2006;**99**:124111.
31. Noblanc O, Gaucher P, Calvarin G. Structural and dielectric studies of $Pb(Mg_{1/3}Nb_{2/3})O_3$–$PbTiO_3$ ferroelectric solid solutions around the morphotropic boundary. *J Appl Phys* 1996;**79**:4291–7.
32. Novak N, Pirc R, Wencka M, Kutnjak Z. High-resolution calorimetric study of $Pb(Mg_{1/3}Nb_{2/3})O_3$ single crystal. *Phys Rev Lett* 2012;**109**:037601.
33. Xie L, Li YL, Yu R, Cheng ZY, Wei XY, Yao X, et al. Static and dynamic polar nanoregions in relaxor ferroelectric $Ba(Ti_{1-x}Sn_x)O_3$ system at high temperature. *Phys Rev B* 2012;**85**:014118.
34. Viehland D, Jang SJ, Cross LE, Wuttig M. Freezing of the polarization fluctuations in lead magnesium niobate relaxors. *J Appl Phys* 1990;**68**:2916–21.
35. Chu F, Reaney IM, Setter N. Spontaneous (zero-field) relaxor-to-ferroelectric-phase transition in disordered $Pb(Sc_{1/2}Nb_{1/2})O_3$. *J Appl Phys* 1995;**77**:1671–6.
36. Deng GC, Ding AL, Li GR, Zheng XS, Cheng WX, Qiu PS, et al. Martensitelike spontaneous relaxor-normal ferroelectric transformation in $Pb(Zn_{1/3}Nb_{2/3})O_3$–$PbLa(ZrTi)O_3$ system. *J Appl Phys* 2005;**98**:094103.
37. Bobnar V, Kutnjak Z, Pirc R, Blinc R, Levstik A. Crossover from glassy to inhomogeneous-ferroelectric nonlinear dielectric response in relaxor ferroelectrics. *Phys Rev Lett* 2000;**84**:5892–5.
38. Li JF, Dai XH, Chow A, Viehland D. Polarization switching mechanisms and electromechanical properties of La-modified lead zirconate titanate ceramics. *J Mater Res* 1995;**10**:926–38.
39. Bobnar V, Kutnjak Z, Pirc R, Levstik A. Electric-field-temperature phase diagram of the relaxor ferroelectric lanthanum-modified lead zirconate titanate. *Phys Rev B* 1999;**60**:6420–7.
40. Zhang Q, Li ZR, Li F, Xu Z, Yao X. Temperature dependence of dielectric/piezoelectric properties of $(1-x)Bi(Mg_{1/2}Ti_{1/2})O_3$–$xPbTiO_3$ ceramics with an MPB composition. *J Am Ceram Soc* 2010;**93**:3330–4.
41. Zhao XH, Qu WG, He H, Vittayakorn N, Tan XL. Influence of cation order on the electric field-induced phase transition in $Pb(Mg_{1/3}Nb_{2/3})O_3$-based relaxor ferroelectrics. *J Am Ceram Soc* 2006;**89**:202–9.
42. Viola G, Ning HP, Wei XJ, Deluca M, Adomkevicius A, Khaliq J, et al. Dielectric relaxation, lattice dynamics and polarization mechanisms in $Bi_{0.5}Na_{0.5}TiO_3$-based lead-free ceramics. *J Appl Phys* 2013;**114**:014107.
43. Zhao WL, Zuo RZ, Fu J, Shi M. Large strains accompanying field-induced ergodic phase-polar ordered phase transformations in $Bi(Mg_{0.5}Ti_{0.5})O_3$–$PbTiO_3$–$(Bi_{0.5}Na_{0.5})TiO_3$ ternary system. *J Eur Ceram Soc* 2014;**34**:2299–309.
44. Jo W, Granzow T, Aulbach E, Rödel J, Damjanovic D. Origin of the large strain response in $(K_{0.5}Na_{0.5})NbO_3$-modified $(Bi_{0.5}Na_{0.5})TiO_3$–$BaTiO_3$ lead-free piezoceramics. *J Appl Phys* 2009;**105**:094102.
45. Jo W, Daniels J, Damjanovic D, Kleemann W, Rödel J. Two-stage processes of electrically induced-ferroelectric to relaxor transition in $0.94(Bi_{1/2}Na_{1/2})TiO_3$–$0.06BaTiO_3$. *Appl Phys Lett* 2013;**102**:192903.
46. Wang D, Fotinich Y, Carman GP. Influence of temperature on the electromechanical and fatigue behavior of piezoelectric ceramics. *J Appl Phys* 1998;**83**:5342–50.
47. Saito Y, Takao H, Tani T, Nonoyama T, Takatori K, Homma T, et al. Lead-free piezoceramics. *Nature* 2004;**432**:84–7.
48. Wang K, Yao FZ, Jo W, Gobeljic D, Shvartsman VV, Lupascu DC, et al. Temperature-insensitive $(K,Na)NbO_3$-based lead-free piezoactuator ceramics. *Adv Funct Mater* 2013;**23**:4079–86.
49. Perrin C, Menguy N, Suard E, Muller C, Caranoni C, Stepanov A. Neutron diffraction study of the relaxor-ferroelectric phase transition in disordered $Pb(Sc_{1/2}Nb_{1/2})O_3$. *J Phys Condens Matter* 2000;**12**:7523–39.
50. Noheda B, Cox DE, Shirane G, Gao J, Ye ZG. Phase diagram of the ferroelectric relaxor $(1-x)PbMg_{1/3}Nb_{2/3}O_3$–$xPbTiO_3$. *Phys Rev B* 2002;**66**:054104.
51. Westphal V, Kleemann W, Glinchuk MD. Diffuse phase transitions and random-field-induced domain states of the "relaxor" ferroelectric $PbMg_{1/3}Nb_{2/3}O_3$. *Phys Rev Lett* 1992;**68**:847–50.
52. Kim DY, Choi JJ, Kim HE. Birefringence study of the freezing mechanism of lanthanum-modified lead zirconate titanate relaxor ferroelectrics. *J Appl Phys* 2003;**93**:1176–9.